*J. Fluid Mech.* (1992), *vol.* 243, *pp.* 519–539
*Printed in Great Britain*



# Some aspects of bifurcation structure of laminar flow in curved ducts

By HSIAO C. KAO

National Aeronautics and Space Administration, Lewis Research Center, Cleveland, OH 44135, USA

(Received 14 September 1991 and in revised form 3 April 1992)

A bifurcation study is made of laminar flow in curved ducts. The problem is formulated in a curvilinear coordinate system, and the governing equations, after orthogonal mapping is applied, are solved numerically by an iterative finite-difference method. Many computer runs were made with various duct cross-sections ranging from a circle to a square, to learn the transition of bifurcation structure with this change in cross-section and to reconcile the differences between them. In addition, a simpler technique is proposed to generate symmetric four-cell solutions in a circular pipe and a means is put forward to stabilize four-vortex structures in a complete cross-section.

## 1. Introduction and outline of approach

Laminar flow in a curved duct has been a research topic for nearly a century. As a result, a voluminous literature is now available, some of which is summarized in a review article by Berger, Talbot & Yao (1983), including the early work on bifurcation structure of fully developed laminar flow in a curved circular pipe. Since then, the problem of solution bifurcation has attracted considerable attention and added a new facet to an old problem. Since the non-uniqueness of laminar flow in a curved duct is a relatively new topic, not every aspect of the problem is completely known, and the purpose of this study is to close some of these gaps. The question of whether the solution branch of a four-vortex structure is stable without symmetry conditions will also be examined briefly.

Following the original work of Dennis & Ng (1982) and Nandakumar & Masliyah (1982), other papers to appear include Winters & Brindley (1984), Nandakumar, Masliyah, & Law (1985), Yang & Keller, (1986), Winters (1987), Soh (1988), Daskopoulos & Lenhoff (1989), and Goering (1989). Most of these studies were carried out in a half-cross-section with symmetry conditions imposed on the geometric symmetry plane. One exception is Winters' work which includes asymmetric solutions. The present study is also limited mostly to the half-cross-section computations, although some efforts were made to attain solutions in a full domain. Numerical calculations indicate that these four-cell solutions cannot in general be maintained except for some solutions of the so-called intermediate type near the limit point. If for some reason a four-cell structure in a complete cross-section is desirable, its presence can be preserved by means of a short splitter plate at the outer bend. The workability of this device will be demonstrated via numerical examples.

The computational methods used in earlier studies are mostly based on the finite-element, collocation or Fourier series methods together with the continuation

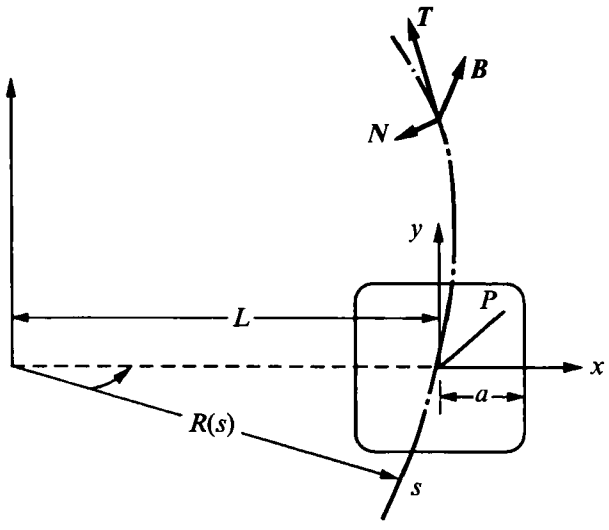


FIGURE 1. Coordinate system.

method by Keller (1977). However, since the most commonly used method for solving the Navier–Stokes equations for flow in a curved pipe is the finite-difference method based on iteration, it will be convenient if the same computational method can be used to study the non-uniqueness of solutions. This procedure is found to be feasible and will be discussed later. There are, however, disadvantages, such as only stable solutions can be obtained by the present method, and a precise prediction of singular points is not possible because the convergence of an iteration procedure at such point is not defined.

The flow in a curved square duct undergoes a transition from a two-cell structure to a four-cell structure automatically as the Dean number increases above a certain critical value. Thus, finding the second family of solutions requires no special effort. In a curved circular pipe, unlike in a square duct, this transition does not take place spontaneously and the primary solutions of a two-cell structure do not terminate. Thus some procedure has to be found to generate at least one solution in another family. (Singular points in a bifurcation diagram can be located by more rigorous methods to connect different branches. See, for example, Yang & Keller 1986 or Winters 1987.) Once this solution is available, it can be used as a starting profile for others. The procedure proposed by Nandakumar & Masliyah (1982) is very useful and gives, in fact, the earliest example of dual solutions in a curved circular pipe by a systematic means. We come across another method, which can also generate a dual solution and will be discussed later.

The state diagram plotted by Winters for a curved square duct includes several families of solutions. If we exclude the branch for asymmetric solutions and the disconnected branch for symmetric solutions, the remaining curve comprises the usual two-cell and four-cell solutions with two limit points and the intermediate solutions connecting them. The characteristics of this curve are different from those given by Daskopoulos & Lenhoff, which seems to imply that the pattern of a state diagram is a function of duct geometry. One purpose of the present study is, therefore, to investigate the transition of the solution structure from a curved square duct to a curved circular pipe. Thus, intermediate geometries are required. The equation described by Roache (1976, p. 302) for a super-ellipse, which changes the

shape smoothly from a circle to a square by varying a single parameter, fulfils this need.

## 2. Governing equations and boundary conditions

The governing differential equations for a steady incompressible fully developed laminar flow in a planar curved duct of arbitrary cross-section are to be derived here. The coordinate system is depicted in figure 1. The centreline of the duct is referred to as $s$, along which there are three unit vectors. The tangent and normal vectors $\boldsymbol{T}$ and $\boldsymbol{N}$ are functions of $s$, while the binormal vector $\boldsymbol{B}$ is independent of $s$. The duct cross-section, which is perpendicular to the centreline, is defined by the coordinates $x$ and $y$ with the origin at duct centre. A point $P$ in the duct is given by a position vector

$$\boldsymbol{P} = \boldsymbol{R}(s) - x(\xi,\eta)\,\boldsymbol{N}(s) + y(\xi,\eta)\,\boldsymbol{B}(s),$$

where $\xi$ and $\eta$ are the boundary-conforming curvilinear coordinates to be obtained through mapping.

Using the Serret–Frenet equations of a two-dimensional curve,

$$\frac{\mathrm{d}\boldsymbol{R}}{\mathrm{d}s} = \boldsymbol{T}, \quad \frac{\mathrm{d}\boldsymbol{N}}{\mathrm{d}s} = -\frac{1}{L}\boldsymbol{T}, \quad \frac{\mathrm{d}\boldsymbol{B}}{\mathrm{d}s} = 0,$$

we have

$$\mathrm{d}\boldsymbol{P} = \frac{\partial \boldsymbol{P}}{\partial s}\mathrm{d}s + \frac{\partial \boldsymbol{P}}{\partial \xi}\mathrm{d}\xi + \frac{\partial \boldsymbol{P}}{\partial \eta}\mathrm{d}\eta = \left(1+\frac{x}{L}\right)\mathrm{d}s\,\boldsymbol{T} + \mathrm{d}\xi\,\boldsymbol{a}_\xi + \mathrm{d}\eta\,\boldsymbol{a}_\eta,$$

where $L$ is the radius of curvature of $s$, and $\boldsymbol{a}_\xi$ and $\boldsymbol{a}_\eta$ are two vectors defined as

$$\boldsymbol{a}_\xi = -\frac{\partial x}{\partial \xi}\boldsymbol{N} + \frac{\partial y}{\partial \xi}\boldsymbol{B}, \quad \boldsymbol{a}_\eta = -\frac{\partial x}{\partial \eta}\boldsymbol{N} + \frac{\partial y}{\partial \eta}\boldsymbol{B}.$$

The triad $\boldsymbol{T}$, $\boldsymbol{a}_\xi$ and $\boldsymbol{a}_\eta$ can be made mutually perpendicular, if the following condition is imposed:

$$\boldsymbol{a}_\xi \cdot \boldsymbol{a}_\eta = \frac{\partial x}{\partial \xi}\frac{\partial x}{\partial \eta} + \frac{\partial y}{\partial \xi}\frac{\partial y}{\partial \eta} = 0,$$

which is recognized to be the metric coefficient $g_{12} = 0$. In other words, if the governing equations are expressible in an orthogonal coordinate system $s$, $\xi$ and $\eta$, an orthogonal mapping between $x$, $y$ and $\xi$, $\eta$ is necessary. Given this condition and taking the scalar product, we obtain

$$\mathrm{d}\boldsymbol{P}\cdot\mathrm{d}\boldsymbol{P} = h_3^2\,\mathrm{d}s^2 + h_1^2\,\mathrm{d}\xi^2 + h_2^2\,\mathrm{d}\eta^2,$$

where $h_1$, $h_2$, and $h_3$ are the usual notation for metric coefficients given by

$$h_1^2 = \left(\frac{\partial x}{\partial \xi}\right)^2 + \left(\frac{\partial y}{\partial \xi}\right)^2, \quad h_2^2 = \left(\frac{\partial x}{\partial \eta}\right)^2 + \left(\frac{\partial y}{\partial \eta}\right)^2, \quad h_3^2 = \left(1+\frac{x}{L}\right)^2.$$

With the orthogonal metrics available, the Navier–Stokes equations in coordinates $s$, $\xi$ and $\eta$ reduce to

$$\frac{\partial}{\partial \xi}(h_2 h_3 U) + \frac{\partial}{\partial \eta}(h_1 h_3 V) = 0, \tag{1}$$

$$\mathrm{D}'U + \frac{V}{h_1 h_2}E' - \frac{W^2}{h_1 h_3}\frac{\partial h_3}{\partial \xi} = -\frac{1}{\rho h_1}\frac{\partial p}{\partial \xi} + \frac{\nu}{h_2 h_3}\frac{\partial}{\partial \eta}H', \tag{2}$$

$$\mathrm{D}'V-\frac{U}{h_1h_2}E'-\frac{W^2}{h_1h_3}\frac{\partial h_3}{\partial\eta}=-\frac{1}{\rho h_2}\frac{\partial p}{\partial\eta}-\frac{\nu}{h_1h_3}\frac{\partial}{\partial\xi}H', \tag{3}$$

$$\mathrm{D}'W+W\left(\frac{U}{h_1h_3}\frac{\partial h_3}{\partial\xi}+\frac{V}{h_2h_3}\frac{\partial h_3}{\partial\eta}\right)$$
$$=-\frac{1}{\rho h_3}\frac{\partial p}{\partial s}+\frac{\nu}{h_1h_2}\left\{\frac{\partial}{\partial\xi}\left[\frac{h_2}{h_1h_3}\frac{\partial}{\partial\xi}(h_3W)\right]+\frac{\partial}{\partial\eta}\left[\frac{h_1}{h_2h_3}\frac{\partial}{\partial\eta}(h_3W)\right]\right\}. \tag{4}$$

Equation (1) is the continuity equation and (2)–(4) are the momentum equations. In these equations $U$, $V$ and $W$ are the velocity components in the $\boldsymbol{a}_\xi$, $\boldsymbol{a}_\eta$ and $\boldsymbol{T}$ directions, $p$ is the pressure, $\rho$ the density, and $\nu$ the kinematic viscosity of the fluid. D′, $E'$ and $H'$ denote

$$\mathrm{D}'=\frac{U}{h_1}\frac{\partial}{\partial\xi}+\frac{V}{h_2}\frac{\partial}{\partial\eta},\quad E'=U\frac{\partial h_1}{\partial\eta}-V\frac{\partial h_2}{\partial\xi},\quad H'=\frac{h_3}{h_1h_2}\left[\frac{\partial}{\partial\eta}(h_1U)-\frac{\partial}{\partial\xi}(h_2V)\right].$$

In deriving these equations, the flow quantities are assumed to be independent of $s$, except $p$ which assumes the following form:

$$p=-Gs+p'(\xi,\eta),$$

where $G$ denotes the constant pressure gradient in the streamwise direction.

The above equations can be substantially simplified by introducing a stream function and by eliminating the pressure, resulting in a vorticity equation. These vorticity–stream function equations, written in dimensionless form, become

$$\Delta'\psi-\epsilon\left[\frac{\partial}{\partial\xi}\left(\omega\frac{\partial y}{\partial\eta}\psi\right)-\frac{\partial}{\partial\eta}\left(\omega\frac{\partial y}{\partial\xi}\psi\right)\right]-\epsilon^2\omega^2h_1h_2\psi=-\frac{h_1h_2}{\omega}\Omega, \tag{5}$$

$$\Delta'w-\left[\frac{\partial}{\partial\xi}\left(\omega\frac{\partial\psi}{\partial\eta}w\right)-\frac{\partial}{\partial\eta}\left(\omega\frac{\partial\psi}{\partial\xi}w\right)\right]+\epsilon\left[\frac{\partial}{\partial\xi}\left(\omega\frac{\partial y}{\partial\eta}w\right)-\frac{\partial}{\partial\eta}\left(\omega\frac{\partial y}{\partial\xi}w\right)\right]$$
$$+2\epsilon\left[\frac{\partial}{\partial\xi}\left(\omega^2\frac{\partial x}{\partial\eta}\psi\right)-\frac{\partial}{\partial\eta}\left(\omega^2\frac{\partial x}{\partial\xi}\psi\right)\right]w=-\omega h_1h_2D, \tag{6}$$

$$\Delta'\Omega-\left[\frac{\partial}{\partial\xi}\left(\omega\frac{\partial\psi}{\partial\eta}\Omega\right)-\frac{\partial}{\partial\eta}\left(\omega\frac{\partial\psi}{\partial\xi}\Omega\right)\right]+\epsilon\left[\frac{\partial}{\partial\xi}\left(\omega\frac{\partial y}{\partial\eta}\Omega\right)-\frac{\partial}{\partial\eta}\left(\omega\frac{\partial y}{\partial\xi}\Omega\right)\right]$$
$$=\frac{1}{2}\left[-\frac{\partial}{\partial\xi}\left(\omega\frac{\partial x}{\partial\eta}w^2\right)+\frac{\partial}{\partial\eta}\left(\omega\frac{\partial x}{\partial\xi}w^2\right)\right], \tag{7}$$

where $\psi$ is the stream function, $\Omega$ the vorticity, and $D$ the Dean number. The symbols $\Delta'$, $\epsilon$ and $\omega$ are given by

$$\Delta'=\frac{\partial}{\partial\xi}\left(\frac{h_2}{h_1}\frac{\partial}{\partial\xi}\right)+\frac{\partial}{\partial\eta}\left(\frac{h_1}{h_2}\frac{\partial}{\partial\eta}\right),\quad \epsilon=\frac{a}{L},\quad \omega=\frac{1}{1+\epsilon x},$$

and other dimensionless quantities are

$$u=\frac{a}{\nu}U=\frac{1}{h_2h_3}\frac{\partial\psi}{\partial\eta},\quad v=\frac{a}{\nu}V=-\frac{1}{h_1h_3}\frac{\partial\psi}{\partial\xi},\quad w=\left(\frac{2a}{L}\right)^{\frac{1}{2}}\frac{a}{\nu}W,$$

$$\Omega=\frac{1}{h_1h_2}\left[\frac{\partial}{\partial\xi}(h_2v)-\frac{\partial}{\partial\eta}(h_1u)\right],\quad D=\frac{Ga^3}{\rho\nu^2}\left(\frac{2a}{L}\right)^{\frac{1}{2}}.$$

Note that all length-related quantities, such as $x$, $\xi$, $h_2 \ldots$, though denoted by the same symbols, are made dimensionless by referring to the 'radius' $a$ (figure 1), except $h_1$ and $\eta$ which are already dimensionless (see §3).

As in a polar coordinate system, (5)–(7) are singular at the origin because the metric coefficient $h_2$ will vanish there. Thus, these equations are recast in local Cartesian coordinates there. This singularity also occurs in the process of mapping, and will be discussed in §3.

To these equations, we add the boundary conditions

$$\psi = \frac{\partial \psi}{\partial \xi} = w = 0, \quad \Omega = -\frac{1}{h_1^2 h_3} \frac{\partial^2 \psi}{\partial \xi^2}$$

at $\xi = 1$, i.e. the duct surface. The condition $\partial \psi / \partial \xi = 0$, which ensures that $v = 0$ at the duct surface, is implemented implicitly in deriving the boundary condition for $\Omega$. This is a common practice, for (5) is solved as a Dirichlet problem. An exception is Greenspan's (1973) computation in which it is imposed explicitly, and the system is then over specified. Our experience, after some experimental computations, seems to indicate that this extra boundary condition will at least hamper convergence, and may cause slow divergence, especially for non-circular cross-sections. For this reason, no further attempts were made in this respect.

For the half-cross-section computations, symmetry conditions are specified on the geometric symmetry plane. These are

$$\psi(x, y) = -\psi(x, -y), \quad \Omega(x, y) = -\Omega(x, -y), \quad w(x, y) = w(x, -y) \tag{8}$$

where $x$ and $y$ are the coordinates in figure 1.

## 3. Orthogonal mapping

As mentioned earlier, one can represent the governing Navier–Stokes equations for a curved duct in an orthogonal coordinate system, provided that there is an orthogonal transformation between $x, y$ and $\xi, \eta$. Here, we further require that this transformation be boundary-conforming, and we assume that curved ducts all have 'super-circular' cross-sections. A super-circle is defined by (Roache 1976, p. 302)

$$(x/a)^n + (y/a)^n = 1, \quad 1 < n < \infty, \tag{9}$$

where $a$ is the 'radius' and $n$ is a positive parameter but not necessarily an integer. In order to see the change from a circle ($n = 2$) to a square ($n \to \infty$), several configurations are plotted in figure 2. As $n$ increases, the configuration becomes fuller and eventually approaches a square with almost sharp corners, whereas as $n$ decreases the configuration becomes thinner and approaches a rhombus in the limit $n = 1$.

To construct a boundary-conforming orthogonal grid in super-circles, the weak-constraint form of Ryskin & Leal's (1983) method is used. The basic method has been described well in their paper and thus we only need add a few points relevant to this problem not included in their paper.

The grid is constructed in a quarter-domain with symmetry conditions imposed on the horizontal and vertical axes. This is chosen because, according to Chikhliwala & Yortsos (1985), symmetry promotes accuracy, and coordinate nodes are specified along all boundaries, including a small circle surrounding the origin. This small circle is to exclude the singularity at the origin. The $\xi$-coordinate varies from zero at the

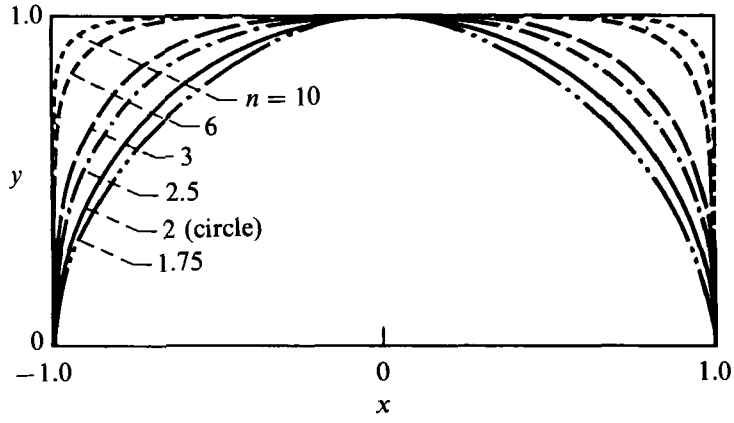


FIGURE 2. Depiction of super-circles of various exponents.

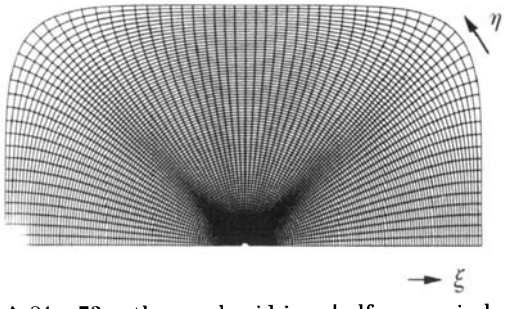


FIGURE 3. A 81 × 73 orthogonal grid in a half-super-circle of $n = 6$.

origin to unity at the boundary which is equally divided in the transformed plane, while the $\eta$-coordinate corresponding approximately to the angle in the polar coordinates, varies from zero at the horizontal axis to $\frac{1}{2}\pi$ at the vertical axis, which is also equally divided. The orthogonality of grid lines is examined by evaluating the intersection angle of two grid lines. For $n \leqslant 6$, the maximum departure from orthogonality in a 81 × 37 quarter-domain grid is about 0.7°. As $n$ increases, the error also increases because relatively sharp corners begin to form. This deterioration can be controlled if more mesh points are placed at the corner. A representative pattern for a 81 × 73 orthogonal grid in a half-domain with $n = 6$ is shown in figure 3.

## 4. Finite-difference procedures

The transformed Navier–Stokes equations ((5)–(7)) are to be solved approximately in a rectangular $(\xi, \eta)$ domain by means of a finite-difference technique, some details of which follow.

Equation (5), which is linear and of the Poisson type with Dirichlet boundary conditions, poses no problem in computation. The dependent variable $\psi$ is approximated by the central difference and the matrix of the resulting algebraic equation along each line is tridiagonal, which is solved by the line-sweeping Thomas algorithm from $\eta = 0$ to $\eta = \pi$ in one direction only.

Equations (6) and (7) are more complex and, in particular, involve convective terms, which cannot be approximated by the central difference but may be

approximated by the quadratic upwind discretization method (QUICK) of Leonard (1979). This practice requires two grid points beyond each computational molecule, instead of one for the central difference, which means that information has to be supplemented beyond the boundary. To avoid this complication, the quadratic interpolation is applied in the interior region two grid points away from the boundary, and the hybrid method of Spalding is used in the space between this region and the boundary.

The finite-difference form for the variable $w$ in (6) in the interior region expressed in common notation is

$$A_{\mathrm{P}} w_{\mathrm{P}} = A_{\mathrm{E}} w_{\mathrm{E}} + A_{\mathrm{W}} w_{\mathrm{W}} + A_{\mathrm{N}} w_{\mathrm{N}} + A_{\mathrm{S}} w_{\mathrm{S}} + A_{\mathrm{EE}} w_{\mathrm{EE}} + A_{\mathrm{WW}} w_{\mathrm{WW}} + A_{\mathrm{NN}} w_{\mathrm{NN}} + A_{\mathrm{SS}} w_{\mathrm{SS}} + S_{\mathrm{u}}.$$

The symbol $w_{\mathrm{P}}$ denotes the discrete value of $w$ at the node point P, which is the centre of a computational molecule, whose faces are placed halfway between P and four neighbouring points. The symbols $w_{\mathrm{E}}$, $w_{\mathrm{W}}$, $w_{\mathrm{N}}$, and $w_{\mathrm{S}}$ are the discrete values of $w$ at the node points to the east, west, north, and south of point P, and $w_{\mathrm{EE}}$ is that of $w$ at the point to the east of the point E. Other quantities $w_{\mathrm{WW}}$, $w_{\mathrm{NN}}$, and $w_{\mathrm{SS}}$ are designated in a similar manner.

The finite-difference coefficients $A_{\mathrm{P}}$, $A_{\mathrm{E}}, \ldots A_{\mathrm{SS}}$ are the results of discretizing the convective and diffusion terms; the symbol $S_{\mathrm{u}}$ denotes the source term. The expressions for these coefficients are fairly long and are not shown here. The procedure is, however, straightforward and the details are available in Huang & Leschziner (1983), including the test to determine the upstream neighbours. The finite-difference form of (7) is attained in a similar manner and assumes a similar form.

The matrix of this algebraic equation along each line is pentadiagonal and thus a line-sweeping pentadiagonal matrix algorithm is used to find solutions for this system. (This algorithm for a pentadiagonal matrix applies equally well for a tridiagonal matrix. Thus no distinction is needed for points next to a solid boundary.) The sweep is carried out in both directions much like the ADI method. Shortly after the QUICK method was introduced, investigators experienced convergence problems and have devised algorithms to overcome them. This turned out to be unnecessary if an alternating-direction sweep is adopted (P. G. Huang 1987, personal communication).

The sequence of computation in one cycle is to solve $\psi$ first and then $w$ and $\Omega$, using the most recent variables available. These variables are under-relaxed in each sweep. The cycle is repeated as necessary, until both the maximum error $\delta$ of local quantities and the relative residuals in the difference equations become sufficiently small.

A maximum error $\delta$ is given by

$$\delta = \max |g_{i,j}^{k} - g_{i,j}^{k-1}|,$$

where $g_{i,j}$ is a local quantity, and $k$ and $k-1$ denote the $k$th and $(k-1)$th iteration. A relative residual is defined by

$$\mathrm{RES} = \sum_{i,j}^{M,N} \frac{|\mathrm{L}(g_{i,j})|}{|g_{i,j}|}, \tag{10}$$

where L is a difference operator to represent the finite-difference forms of (5)–(7), and

the summation is over the entire region with $M$ and $N$ denoting the total grid points in the $\xi$- and $\eta$-directions. Normally iterations terminate if all three relative residuals become less than $5 \times 10^{-6} \sim 5 \times 10^{-5}$. However, convergence becomes less certain as the bifurcation point is neared and the procedure has to be tightened. This point will be discussed later.

In the course of numerical computations, a computer code in the appendix of Sidi (1991) became available and was applied often to accelerate our iterative solutions especially for computations involving a fine grid. This code requires no change of user's program, which is treated merely as a subroutine, and uses the vector acceleration methods such as the reduced rank extrapolation to speed up convergence. No acceleration procedure is, however, applied when the solution is near a singular point for fear of an adverse effect on the final result.

Equations (5)–(7) as shown are not valid at the origin. This singularity is caused by the choice of the coordinate system and can be removed by recasting the equations in a local Cartesian coordinate system. Only the quantity $w$ needs to be determined at the origin in a half-domain, since $\psi$ and $\Omega$ are zero. However, all three have to be determined in a full domain.

## 5. Generation of four-vortex solutions and accuracy comparison

It is well known that the finite-difference method can accurately predict two-cell and four-cell solutions. What is not certain is whether sufficient accuracy will be achieved for solutions near the singular points. To answer this question, we compare the results calculated here with those of Winters (1987), Dennis & Ng (1982), and Daskopoulos & Lenhoff (1989).

Winters' calculation deals with a square duct in which solutions will undergo an abrupt change from two-cell forms to four-cell ones as $D$ increases. Thus, the location of the limit point will appear automatically, at least approximately. Such is, however, not the case for flows in a circular pipe. Four-cell solutions will not normally simply appear as the Dean number increases, and so some means of generating them becomes necessary.

We begin with an accuracy comparison with Winters' results. For this we essentially use Winters' governing equations recast in terms of $\psi$ and $\Omega$, similar to (5)–(7). The critical region where a disagreement may occur is probably in the proximity of singular points. For this reason, we selected Winters' figure 4(*b*) for a detailed comparison (see figure 4). This is a state diagram with two singular points, which depicts the variation of the central axial velocity $\chi_s$ against the axial pressure gradient $q$. The locus corresponding to two-cell solutions is labelled $S_1$ and terminates at the limit point $L_2$, while that corresponding to four-cell solutions is labelled $S_3$ and begins from the limit point $L_1$. A curve $S_2$ that connects these two loci is another branch also corresponding to four-cell solutions but of an 'intermediate' type. For clarity and convenience, we prefer to use Winters' variables. These variables can be converted to the present ones via the formulae

$$\chi_s = \frac{w_0}{(2\epsilon)^{\frac{1}{2}}}, \quad q = \frac{D}{(2\epsilon)^{\frac{1}{2}}},$$

where $w_0$ denotes the axial velocity at the origin. The curvature $\epsilon$ in these calculations is equal to 0.02. The present solutions are plotted in figure 4 as symbols and Winters' as lines.

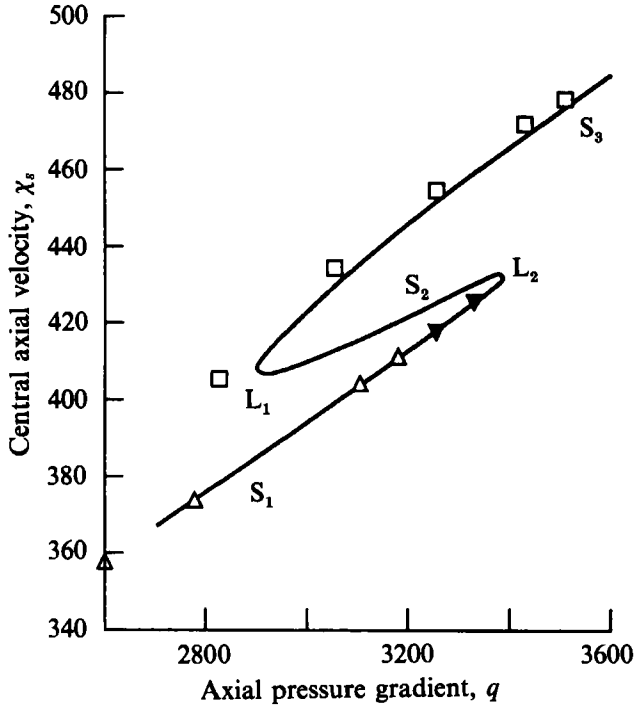


FIGURE 4. Comparison with Winters' state diagram: ——, Winters' curve; △, present two-cell solutions; ▼, present intermediate-type solutions; □, present four-cell solutions.

The agreement at first glance is seen to be very good, especially along $S_1$. There are, however, two differences: (*a*) The limit points $L_1$ and $L_2$ were not predicted precisely. This is expected, since the present method will cease to function at or even near a singular point. (*b*) A close look at figure 4 reveals that there are two solid symbols along curve $S_1$, whose secondary flows involve two pairs of vortices of which the second pair is small and extremely weak. According to Winters' classification, these are of the intermediate type and should be situated on $S_2$ instead of $S_1$. This shift of the intermediate-type solutions to the locus of two-cell structure was also observed by Soh (1988). The overall agreement appears, however, to be reasonable.

All the present solutions shown in figure 4 were computed in a $81 \times 41$ grid in a half-domain with symmetry conditions imposed on the symmetry plane. A coarser grid, $41 \times 21$, can predict fairly accurate results away from singular points but near them a finer grid is needed. The probable reason is that the transformation from a two-cell pattern to a four-cell one (and vice versa) takes place slowly in an iteration process. The incipiency of the secondary pair usually occurs in a small area at the outer bend, and a coarse grid will conceivably hinder its development.

In Winters' state diagram for a square duct, there are two disconnected solution loci for symmetric two-cell and four-cell solutions at somewhat higher Dean numbers than those in figure 4. Originally it was thought that we might leap over from $S_1$ or $S_3$ to these solutions by using the so-called secant predictor. This turned out to be unworkable; these solutions, though symmetric, may be of a different type and could not be reached by the secant predictor used in this study.

We next turn our attention to the flow in a curved circular pipe. As indicated earlier, it is not a trivial matter to secure the first four-cell solution. The usual

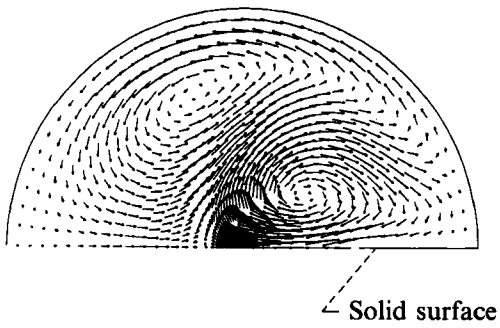


FIGURE 5. Cross-flow vectors of a four-cell solution in a half-domain with a solid surface replacing a portion of the line of symmetry.

procedure, short of an unexpected emergence as happened to Dennis & Ng, is the one proposed by Nandakuma & Masliyah (1982). Another procedure, which can give a four-cell solution, is as follows. This procedure is based on an observation that solutions in a half-domain with symmetry conditions imposed everywhere on the symmetry plane except a portion of it at the outer bend, possess four-cell structures (figure 5). This property can now be utilized to produce a four-cell solution. In the present procedure, the steps are as follows. (*a*) A two-cell symmetric solution is assumed to be available at a Dean number sufficiently high ($D = 2000$ for example) for a four-cell solution to prevail. (*b*) Change a portion of the symmetry plane at the outer bend from symmetry conditions to a solid surface; perform calculation by iteration. In this manner a four-cell solution will gradually emerge. Stop the computation when it becomes nearly convergent. (*c*) Change this portion from a solid boundary to symmetry conditions and carry out the computation as usual until convergence is reached. Our experience shows that the four-cell solution obtained in step (*b*) will undergo adjustment but will not revert to a two-cell structure.

The availability of this solution enables us to make use of the so-called secant predictor method to extend the locus for four-cell solutions. In these calculations, terms of $O(\epsilon)$ and higher in (5)–(7) were neglected in agreement with the assumptions made by Dennis & Ng (1982) and Daskopoulos & Lenhoff (1982). To calculate the friction ratio, it is convenient to define a mean axial velocity written in the generalized coordinates as

$$\bar{w} = \frac{\iint w h_1 h_2 \, \mathrm{d}\xi \, \mathrm{d}\eta}{\iint h_1 h_2 \, \mathrm{d}\xi \, \mathrm{d}\eta}.$$

The friction ratio defined by Dennis & Ng can now be written as

$$\frac{\gamma_c}{\gamma_s} = \frac{D}{8\bar{w}},$$

where the subscripts c and s denote curved and straight pipe respectively. Comparison of this friction ratio between the present calculation and theirs is shown in table 1.

In obtaining the present results, the grid used is basically of $81 \times 37$ points in a half-domain, except for two runs for the four-cell solutions. This basic grid, having

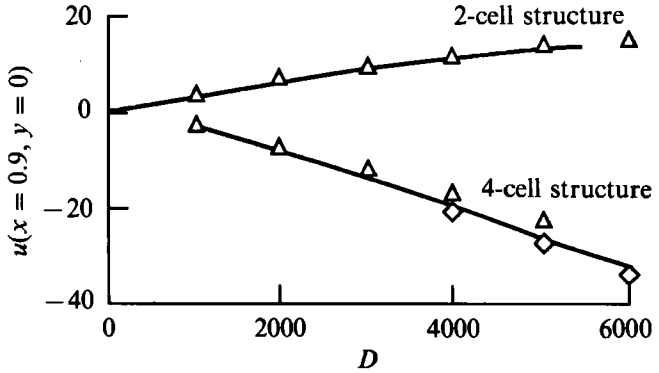


FIGURE 6. Comparison of Daskopoulos & Lenhoff's (1982) state diagram (——) with the present solutions (△, 81 × 37 grid; ◇, 81 × 73 grid).

| | $\frac{\gamma_c}{\gamma_s}$ (two-cell solution) | | $\frac{\gamma_c}{\gamma_s}$ (four-cell solution) | |
|---|---|---|---|---|
| $D$ | Dennis & Ng | Present | Dennis & Ng | Present |
| 1000 | 1.548 | 1.548 | 1.548 | 1.546 |
| 2000 | 1.847 | 1.844 | 1.833 | 1.829 |
| 3000 | 2.064 | 2.060 | 2.046 | 2.042 |
| 4000 | 2.237 | 2.231 | 2.218 | 2.216 |
| 5000 | 2.377 | 2.375 | 2.366 | 2.364 |

TABLE 1. Comparison of friction ratios

only 37 points in the $\eta$-direction (circumferential), is too sparse, especially for four-cell structures. A finer spacing is needed, as will become more evident later. The test for termination of computation is usually RES $\leqslant 5 \times 10^{-5}$. The agreement shown in this table is seen to be reasonable, although almost every predicted friction ratio in the present computation is somewhat lower than its counterpart from Dennis & Ng.

In view of the fact that a friction ratio represents merely a global property of the flow and lacks sensitivity to local variations, any discrepancy will probably show up more in a state diagram. For this reason, we next consider in figure 6 Daskopoulos & Lenhoff's plot. Again we use their coordinate system and place the present data points over their solutions loci. These points are taken from the same computer runs used for table 1; the state variable shown is the velocity component $u$ at $x = 0.9$ and $y = 0$, the choice of Daskopoulos & Lenhoff.

As seen, the agreement for the two-cell solutions appears to be very good. However, our predicted state variables for the four-cell solutions are all somewhat higher than their locus and become progressively worse as $D$ increases. We attribute this to the insufficient number of grid points in the $\eta$-direction (5° intervals). To show that this is the case, three runs at $D = 4000$, 5000, and 6000 were repeated using a $81 \times 73$ grid instead of the usual $81 \times 37$ one and are depicted as diamonds in figure 6. The agreement is improved. Thus, is appears that there is a need for a fine grid when $D$ becomes large.

It seems clear from figure 6 that two solution loci will meet somewhere in the region $0 < D < 1000$, their intersection being the limit point. The actual process of

locating a branching point on a solution locus in this case by an iterative procedure, even approximately, is not easy, because there is no abrupt jump from one solution to another. The main difficulties are that not only is an iterative procedure not defined at or even near a singular point, but a secondary (four-cell) solution near the branching point is 'unstable' and will switch prematurely to a primary (two-cell) solution due presumably to a small disturbance. Moreover, the incipiency of the switch process also depends upon the test for the relative residual for termination (RES). For instance, if RES $\leqslant 4 \times 10^{-5}$, the switch will take place at $957 < D < 959$. As RES increases (decreases), the switch will occur somewhat later (sooner). (The upper bound here for $D$ implies that at this value the solution is a four-cell structure, but as $D$ is reduced in one downward step to the lower bound it becomes a two-cell solution.) The inability to locate precisely the limit point is a deficiency of this procedure, but should not seriously hamper our attempt to investigate the process of solution transition in the change in cross-section from a circle to a square. We will demonstrate in the next section that this transition takes place fairly rapidly as the geometry evolves from nearly circular ($n = 2.5$) to circular ($n = 2$).

## 6. Curved duct of super-circular cross-section

We have seen so far two types of bifurcation in a curved duct. The first is exemplified by figure 6 for a circular pipe, and the second by figures 4 or 7 for a square duct with the presence of a hysteresis. (For convenience, the occurrence of a jump and a double-valued appearance in a state diagram is referred to as hysteresis here.) Two questions may now be raised: whether there exists a relationship between these two types of flow, and, if this relationship exists, how they are related. In this and the next sections we make an attempt to answer them by constructing a family of solution loci for various super-circular shapes ranging from a circle to a near square. The disposition of these curves will then reveal the nature of this problem.

The configurations in this series of computations vary from $n = 10$ to 1.75 including $n = 2$, where $n$ is the exponent in (9). The Dean numbers vary from 300 to 5000. If hysteresis exists, some Dean numbers may be repeated for both two-cell and four-cell solutions. To initiate a calculation for a new index $n$, we need a starting profile which is obtained by transferring a known solution at a neighbouring $n$ to the grid of the desired $n$, whose $D$ value is kept the same and chosen to be not near the singularity. Three different grid distributions are used in the computations. The $81 \times 37$ grid is most often used for calculation of two-cell solutions, while the $41 \times 73$ or $81 \times 73$ grid is generally used for four-cell solutions. If the calculation is near a limit point, we always use the finest grid, $81 \times 73$. The curvature ratio $\epsilon$ for every calculation in this series is, however, fixed at $\epsilon = 0.02$ (Winters' choice) to make comparisons less ambiguous.

Since this series comprises a large number of computer runs, only a few are selected for discussion. One of these is a super-circular cross-section duct of $n = 10$, denoted a pw 10 duct; there are similar designations for other shapes. Since this closely resembles a square duct apart from the corners, one expects that there are also similarities in flow properties, and the state diagram in figure 7 convinces us that such is the case. Notice that the state variable in this figure is chosen to be the velocity component $u$ at $x = 0.9$ and $y = 0$ as in figure 6 instead of $\chi_s$, since it is felt that the former is a more responsive variable.

Next we select three representative cases in a pw 10 duct and show their flow patterns in figure 8. These are a two-cell, an intermediate-type and a four-cell

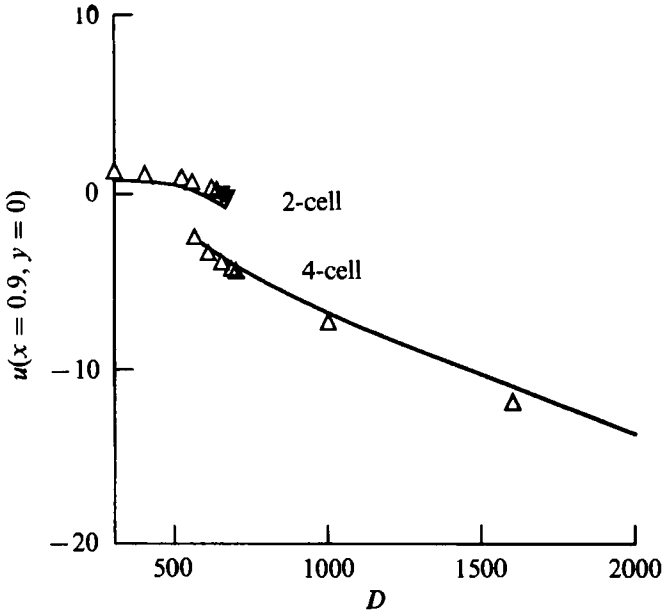


FIGURE 7. State diagram for a square duct (△), a square duct intermediate type (▼) and pw 10 duct (super-circle of $n = 10$) (——).

solution. Here and hereafter we usually illustrate the secondary flows by plotting velocity vectors projected on the cross-sectional plane and scale them to fit the figure. For instance, the same scaling factor is used for figures 8(*a*), 8(*c*) and 8(*e*) to bring out the swiftness of the motion at a higher Dean number, with the exception of the velocity vectors in the second pair of vortices in figure 8(*c*): their magnitudes have been increased eightfold because, being of an intermediate type, they are very weak, nearly motionless and not discerned easily without a local magnification.

We now make an attempt to interpret some properties observed in figure 8. The general appearance of figure 8(*a*) is similar to that for a two-cell solution in a curved circular pipe with the centre of the vortex situated almost directly above the origin, a characteristic feature for low-Dean-number flows. As usual, this pair of counter-rotating vortices alters the pattern of axial velocity contours in figure 8(*b*). The high-velocity region is shifted outward to the outer bend and squashed to look like a kidney with twin peak velocities, one in each half, instead of the single peak in a straight pw 10 duct. The magnitude of these two peak velocities is less than that in a corresponding straight duct (table 2).

Figures 8(*c*) and 8(*d*) illustrate the cross-flow vectors and $w$ contour lines at $D = 640$, for an intermediate-type solution, defined to be a solution whose state variable lies along the locus for two-cell solutions (figure 7) and yet possesses two pairs of vortices in the cross-flow plane, where the second pair is extremely weak.

The flow patterns in figures 8(*e*) and 8(*f*) with $D = 3000$ have the most striking features. Both pairs of vortices are now of nearly equal strength with the second pair occupying a fairly large area at the outer bend. Two swiftly moving currents exists at the interfaces to divide two counter-rotating cells. The first pair of vortices moves further inward and upward to cause isovelocity contours in figure 8(*f*) to make sharp turns in the second quadrant. Because of the high intensity of the second pair, those kidney-shaped high-velocity regions observed in figures 8(*b*) and 8(*d*) can no longer

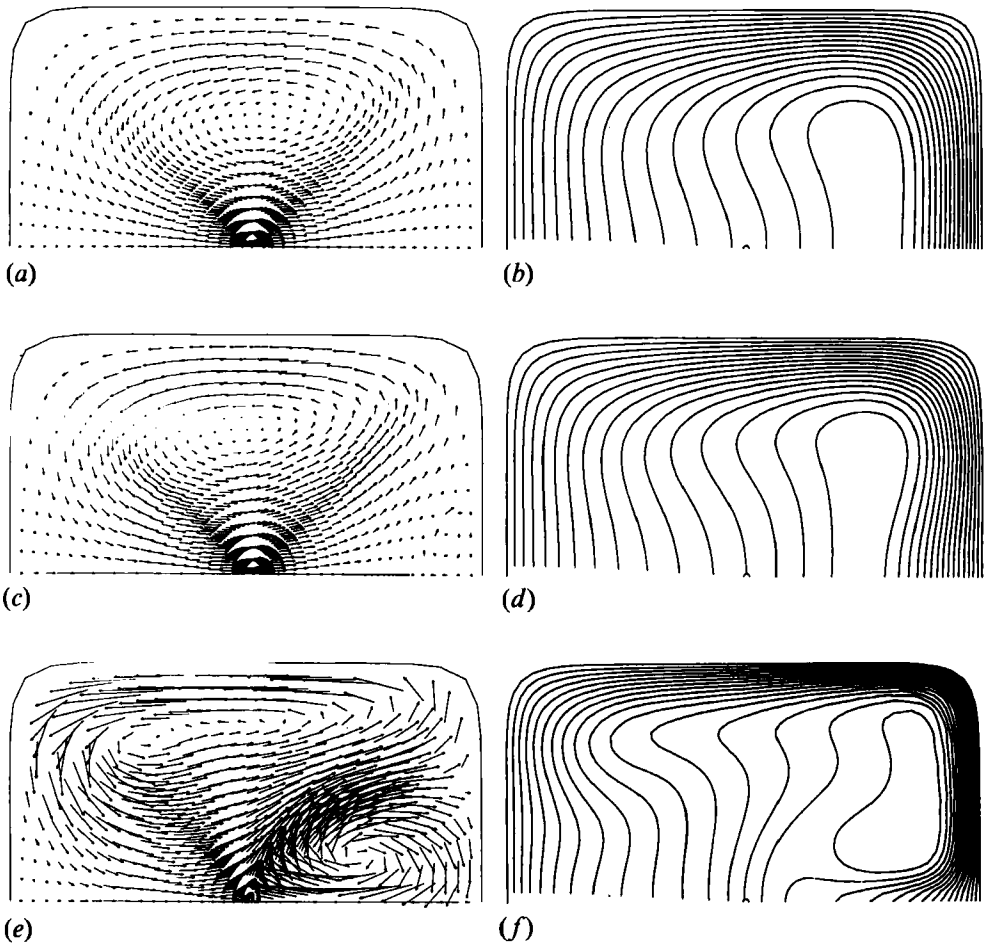


FIGURE 8. Cross-flow vectors and axial velocity contours for three representative solutions in a curved pw 10 duct. (*a*), (*b*) Two-cell solution at $D = 400$; (*c*), (*d*) Intermediate-type solution at $D = 640$; (*e*), (*f*) Four-cell solution at $D = 3000$. (Contour lines of 16 increments; maximum values: $w_{max} = 77.49$ in (*b*), 110.78 in (*d*), 313.79 in (*f*).)

| | pw 10 duct | | | Circular pipe | | |
|---|---|---|---|---|---|---|
| $D$ | $(w_{max})_c$ | $(w_{max})_s$ | $\frac{(w_{max})_c}{(w_{max})_s}$ | $(w_{max})_c$ | $(w_{max})_s$ | $\frac{(w_{max})_c}{(w_{max})_s}$ |
| 300 | 62.59 | 88.33 | 0.709 | 57.75 | 75.0 | 0.770 |
| 500 | 91.84 | 147.21 | 0.624 | 83.49 | 125.0 | 0.668 |
| 1000 | 140.81 | 294.42 | 0.478 | [a]137.00 | 250.0 | 0.548 |
| 3000 | 313.79 | 883.26 | 0.355 | [a]303.70 | 750.0 | 0.405 |
| 5000 | 454.25 | 1472.1 | 0.309 | [a]434.62 | 1250.0 | 0.348 |

[a] Values obtained from four-cell solutions.
Subscripts c and s denote curved and straight respectively.

TABLE 2. Comparison of peak velocities in curved ($\epsilon = 0.02$) and straight pipes

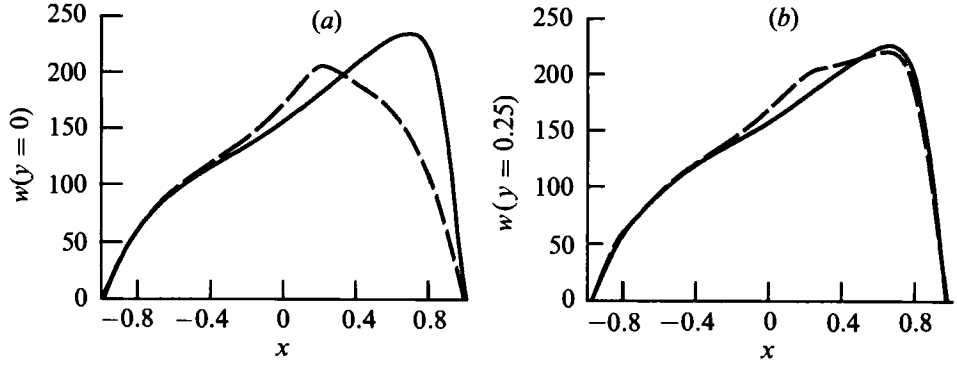


FIGURE 9. Axial velocity profiles in a circular pipe at $D = 2000$: ——, 2-cell; – –, 4-cell. (*a*) $y = 0$, (*b*) $y = 0.25$.

| | | $\bar{w}$ | |
|---|---|---|---|
| Duct shape | $D$ | Two-cell solution | Four-cell solution |
| Circle | 2000 | 135.50 | 136.63 |
| pw 10 | 570 | [a]57.24 | 56.31 |
| Square | 650 | 63.03 | 60.96 |

[a] An intermediate-type solution.

TABLE 3. Comparison of mean axial velocities of two- and four-cell solutions in different pipes ($\epsilon = 0.02$)

be maintained and must bulge sharply inward. The severe contortion of isovelocity contours is perhaps also the cause of a large decrease in peak velocities.

To see the decrease of these peak velocities in curved pipes, some calculated results are listed in table 2. The ratio of peak velocity in a curved pipe to that in a corresponding straight pipe under the same pressure gradient is seen to decrease as $D$ increases, and the descent is steeper at lower Dean numbers than at higher numbers. When comparing to a circular pipe, we find that the decrease in a pw 10 duct is approximately 10% larger than that in a circular pipe.

Normally we would think that the presence of an additional pair of cross-flow vortices would hinder the fluid motion and thus increase the friction. For square or near-square ducts this assumption seems to be correct, and the mean axial velocities in table 3 bear this out. Unfortunately the computed results for a circular pipe belie this assumption as shown here and also in table 1. We feel that this reverse trend is hard to explain, owing perhaps to an inadequate understanding of the loss mechanisms in secondary flow as indicated by Hawthorne (1990). An attempt is nonetheless made to look for the source of this departure by providing several profiles in figure 9.

There are two $w$-profiles plotted along the symmetric axis, $y = 0$, in figure 9(*a*); the dashed line is for the four-cell solution at $D = 2000$, whose integrated area is seen to be smaller than the integrated area of the solid line (two-cell solution also at $D = 2000$). However, as we move away from the symmetric axis, this trend reverses. For instance, the $w$-profiles plotted along $y = 0.25$ in figure 9(*b*) (a horizontal line at a $\frac{1}{4}$ distance above the symmetric axis) indicate that the integrated area of the dashed

line is now somewhat larger than that of the solid line. When $y > 0.25$, this trend is found to persist. Thus, it is conceivable that the total integrated area for the dashed lines eventually becomes larger than that for the solid line in spite of a large deficit near the symmetric axis. If similar profiles are plotted for solutions in a square duct at $D = 570$, no such reversal is detected.

## 7. Transition of solution structure

We now consider one of the main aspects of this study, shown in the composite state diagram in figure 10. The configurations in this diagram range from a near square ($n = 10$) to a pw 1.75 duct ($n = 1.75$) and the Dean numbers range from 300 to 5000. Because of the solution structure, some loci will terminate prior to $D = 5000$ (the disappearance of two-cell solutions), and others may not begin until $D > 300$ (the non-existence of four-cell solutions). Notice that no computer runs were made in the range $D = 0$ to 300.

In the group of two-cell solutions one observes that the solution loci for the pw 10, pw 3 and pw 2.5 ducts all terminate at $D < 5000$, but as $n$ decreases the locus lengthens, which means that the hysteresis region expands. This process of expansion is, however, very slow between $n = 10$ and $n = 3$ in contrast to the fairly rapid change of geometry in this range. Even at $n = 2.5$, which is rather similar to a circle, the two-cell solution terminates at $D \approx 4250$. However, as soon as $n$ becomes 2, the extent of two-cell solutions is much expanded and continues to $D = 30000$ at least (Soh & Berger 1987). This sudden expansion may be construed as evidence that the flow process undergoes a morphogenesis, evolving from one structure to another through a transcritical bifurcation point at a distinct value of $n$ (a referee's comment). If this process holds, the hysteresis will disappear abruptly at the transcritical point and the solution branches become disconnected, somewhat similar to the bifurcation loci shown in figure 2 or 3 of Schaeffer (1980).

In order to see the flow properties in a cross-section thinner than a circle, we made additional computations in a pw 1.75 duct ($n = 1.75$). As expected, the upward trend for the solution loci continues and it is now above the locus for a circular pipe in figure 10. A higher location of a two-cell locus implies that the velocity vector at $x = 0.9$ on the plane of symmetry for the same Dean number is larger than that of a lower position. This does not, however, imply that the vortex intensity of the former is higher than that of the latter. The opposite may actually be true. The difference appears to come from the disposition of vortices caused by the cross-sectional shape. For instance, the vortex in figure 11 (*a*) is more concentrated than that in figure 11 (*b*). As a result, the velocity components decay faster than those in figure 11 (*b*), resulting in a smaller $u$ at $x = 0.9$ and $y = 0$.

In principle, loci for two-cell solutions will all eventually converge to the point $u = D = 0$. The curves drawn in figure 10 seem to bear this out.

From the group of four-cell solutions one finds that, as $n$ decreases, the solution locus moves to a higher position in the state diagram, and at the same time the estimated Dean number for incipiency of a four-cell solution becomes larger. One also notices that the magnitudes of $u$ at incipient points are almost equal. This is probably due to the inability of the present method to deal with singularities. The present computations for these solutions stopped at $D = 5000$, but the indications are that this is not the upper limit and it can be much higher.

In Winters' analysis for a curved square duct the two-cell solution locus and the four-cell one are connected by another locus shown as $S_2$ in figure 4. Since the pw 10

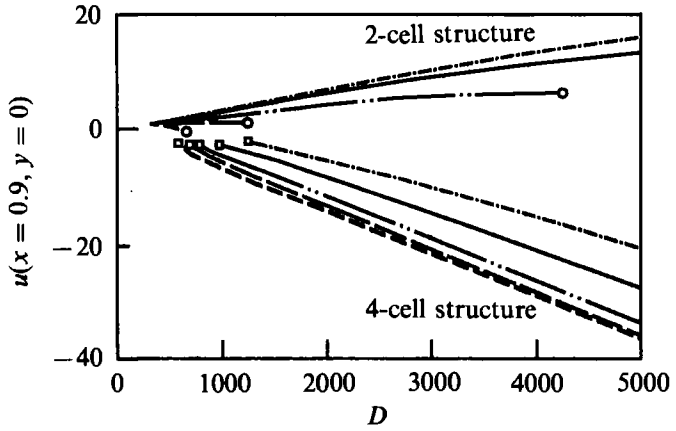


FIGURE 10. State diagram showing solution loci of various cross-sections: ——·——, pw 1.75; ——, pw 2; ——· ·——, pw 2.5; – –, pw 3; - - -, pw 10. □, Incipiency of four-cell solutions; ○, termination of two-cell solutions.

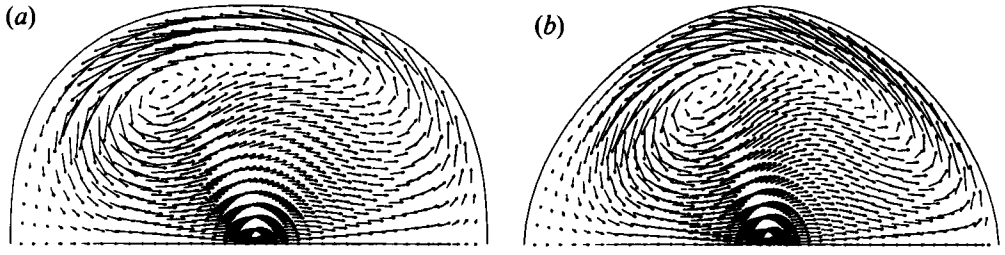


FIGURE 11. Cross-flow velocity vectors of two-cell solutions at $D = 4000$. (*a*) Curved pw 2.5 duct; (*b*) curved pw 1.75 duct.

is a near square configuration, it is assumed that there also exists an intermediate locus similar to $S_2$ in figure 7. However, no such intermediate locus is indicated by Daskopoulos & Lenhoff in a curved circular pipe. This perhaps lends further support to the assumption that the flow process undergoes a morphogenesis at $n \approx 2$.

## 8. Computation in a complete cross-section

All previous solutions are symmetric, obtained in a half-cross-section with symmetry conditions imposed on the centreline. If these conditions are removed and the computation is done in a complete cross-section, it is known that four-cell solutions are unstable (see Goering, Humphrey & Greif 1990, for example). We, of course, experienced the same difficulty, but in the present case these unstable solutions develop slowly. Using a curved circular pipe as an example, the development of an unstable solution is as follows. The initial condition for the computation is the two symmetric four-cell solutions patched together along the centreline. After a number of iterations, asymmetry begins to develop, and the pattern becomes distorted, intensifies and oscillates about the centreline (slosh). This sloshing will eventually subside and a two-cell structure emerges. Incidentally, the word instability here refers to the inability to maintain its original structure and does not imply an uncontrolled growth of solution.

Since it appears that the breakdown begins with a sloshing, a four-cell structure

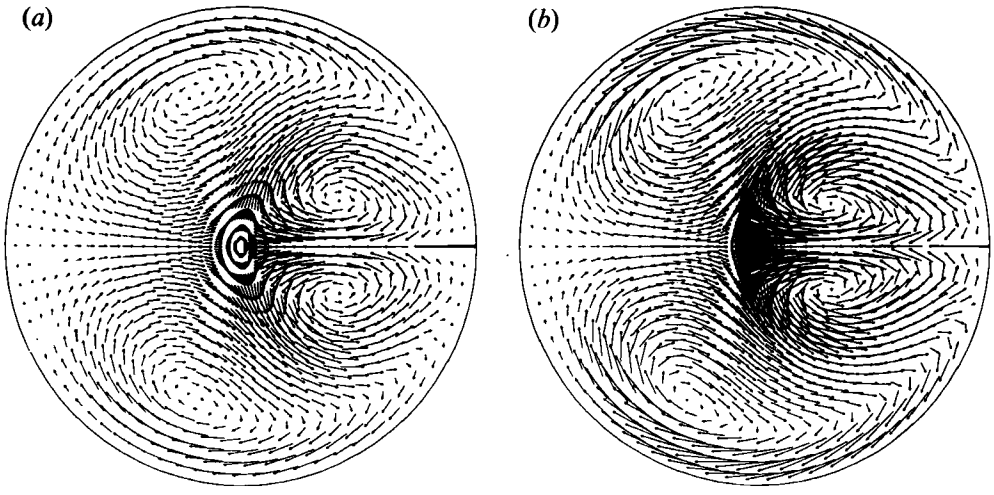


FIGURE 12. Cross-flow velocity vectors in a circular pipe with a splitter plate at the outer bend in the limit of negligible curvature: (a) $D = 2000$; (b) $D = 4000$.

may thus be preserved, if sloshing can be controlled. Based on this assumption, a splitter plate of approximately 15 to 25% of the duct diameter is introduced at the outer bend along the centreline to function as a stabilizer. Several solutions for this configuration with various length of the splitter plate were obtained and two are plotted in figure 12 for $D = 2000$ and 4000. In these two examples the splitter plate measures approximately 15% of the pipe diameter. This length can be increased and the flow pattern will change somewhat, but if it is reduced to about 10% of the diameter, sloshing occurs and computation will not converge.

It is seen in figure 12 that a splitter plate also acts as a means to channel the cross-flow into a jet-like stream, which collides with the return flow from the inner bend. This becomes fairly clear at $D = 4000$. If an agitation of this kind is a desirable feature for enhancing mixing or heat transfer, a splitter plate could be a useful device. The friction coefficient will, however, increase owing to the presence of an additional surface. The increase in these two examples turns out to be also approximately 15% (see figure 14).

It is known that the onset of turbulence is delayed in a curved pipe. This is often attributed to the presence of a secondary flow which enhances mixing and thus retards transition. If this is the primary reason for delaying, it then seems plausible that maintaining a four-vortex structure will further delay transition because of a higher degree of mixing.

A few trial runs for higher Dean numbers were also made. The indications are that as $D$ increases to 5000, a splitter plate of 15% of the duct diameter is no longer capable of controlling sloshing, which persisted throughout the entire iteration process, although there was no emergence of a two-cell structure.

A two-cell solution is known to be stable in a complete cross-section. Our computation based on limited examples seems to show that a solution of the intermediate type is also stable in a complete cross-section.

When the Dean number is small, say $D = 500$, insertion of a short splitter plate does not generally change the flow from a two- to four-cell structure. However, if it is about 1000, both flow structures are possible, depending on the length of the splitter plate.

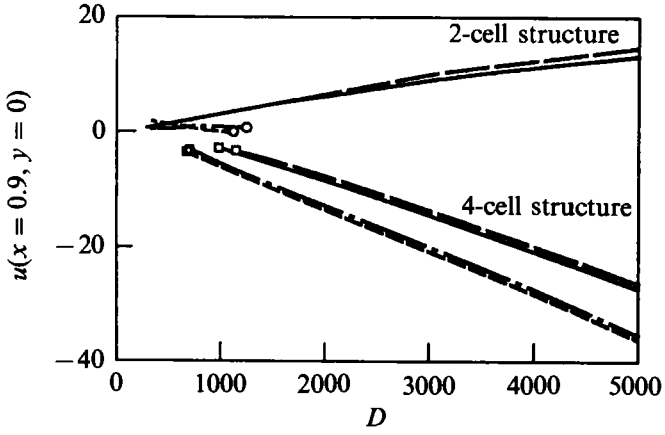


FIGURE 13. Effect of curvature on a state diagram: ○, termination of two-cell solutions; □, incipiency of four-cell solutions. For pw 2: ——, $\epsilon = 0.02$; – –, $\epsilon = 0.2$. For pw 3: – – –, $\epsilon = 0.02$; ——– – ——, $\epsilon = 0.2$.

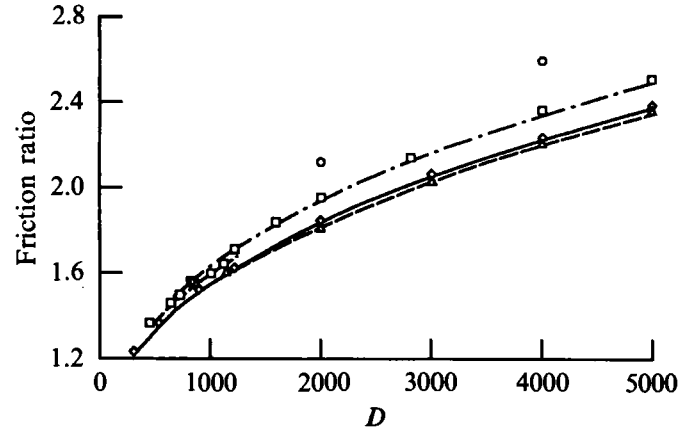


FIGURE 14. Effect of curvature on friction ratios. Lines for $\epsilon = 0.02$ solutions; symbols for $\epsilon = 0.2$ solutions except those with splitter plate: ——, two-cell in pw 2; – – –, four-cell in pw 2; – –, two-cell in pw 3; ——·——, four-cell in pw 3; ◇, two-cell in pw 2; △, four-cell in pw 2; □, two- and four-cell in pw 3; ○, four-cell with splitter plate.

## 9. Effect of curvature

The previous computations were all done with small curvature ratios ($\epsilon = 0$ and 0.02), and so the effect of curvature on the flow properties should be examined, especially with regard to state diagrams. For this reason, computations are also made with $\epsilon = 0.2$ in both circular and pw 3 ducts, and are plotted in figure 13. This figure shows that the curvature effect on the state diagram is apparently small in spite of a tenfold increase in $\epsilon$, though the solution loci with larger $\epsilon$ are all somewhat higher than those with smaller $\epsilon$.

These results also enable us to see the curvature effect on friction ratios, illustrated in figure 14. The usual finding that a curvature exerts only a minor influence on the friction is also evident here. The somewhat unusual property mentioned earlier that the presence of an additional pair of vortices actually increases the flux slightly can now be seen graphically. In addition, one finds that the friction ratio for a circular

pipe is lower than that for a pw 3 duct. (The evidence from a few other computations seems to indicate that a circular pipe has a lower friction ratio than other cross-sections.)

Soh & Berger (1987) among others also investigate the curvature effect on friction ratios in a circular pipe with two-cell solutions. Their examples are for $\epsilon = 0.01$, 0.1 and 0.2. A comparison of the present results with their case of $\epsilon = 0.2$ shows signs of differences, with the present results consistently lower than theirs. For the case of $\epsilon = 0.01$, only an approximate comparison is feasible, because our examples are for $\epsilon = 0$ and $\epsilon = 0.02$. This approximate comparison shows, however, a good agreement.

## 10. Concluding remarks

A study of bifurcation structure from a somewhat different viewpoint is presented here. The governing equations are solved numerically by an iterative finite-difference method, and the solutions are plotted to show the loci in the state diagrams. We examine the transition of the solution structure from a square to a circular duct and reconcile their differences. This effort is, however, limited to one branch of the solution loci among several investigated by Winters. Although other branches are not at present known to exist in a curved circular pipe, it should be of interest to see how they evolve as the geometry changes and whether they all vanish as $n \to 2$. The question of whether four-cell solutions are stable or can be realized experimentally posed by, for example, Goering *et al.* (1990) is only dealt with briefly here; a further investigation would be useful.

It is a pleasure to thank Dr A. Sidi for making his acceleration code available and Dr P. G. Huang for discussions about the QUICK method.

REFERENCES

BERGER, S. A., TALBOT, L. & YAO, L. S. 1983 Flow in curved pipes. *Ann. Rev. Fluid Mech.* **15**, 461–512.

CHIKHLIWALA, E. D. & YORTSOS, Y. C. 1985 Application of orthogonal mapping to some two-dimensional domains. *J. Comput. Phys.* **57**, 391–402.

DASKOPOULOS, P. & LENHOFF, A. M. 1989 Flow in curved ducts: bifurcation structure for stationary ducts. *J. Fluid Mech.* **203**, 125–148.

DENNIS, S. C. R. & NG, M. 1982 Dual solutions for steady laminar flow through a curved tube. *Q. J. Mech. Appl. Maths.* **35**, 305–324.

GOERING, D. J. 1989 The effect of curvature and buoyancy in three-dimensional pipe flows. Ph.D. thesis, University of California Berkeley.

GOERING, J. J., HUMPHREY, J. A. C. & GREIF, R. 1990 Curved pipe flows. Some unanswered questions in fluid mechanics, compiled by L. M. Trefethen & R. L. Panton. *Appl. Mech. Rev.* **43** (8) 153–169.

GREENSPAN, D. 1973 Secondary flow in a curved tube. *J. Fluid Mech.* **57**, 167–176.

HAWTHORNE, W. 1990 Loss mechanisms in secondary flow. Some unanswered questions in fluid mechanics, compiled by L. M. Trefethen & R. L. Panton. *Appl. Mech. Rev.* **43** (8), 153–169.

HUANG, P. G. & LESCHZINER, M. A. 1983 An introduction and guide to the computer code TEAM. *Rep.* TFD/83/9(R). Thermo-fluid Div., Dept. Mech. Engng, Univ. Manchester Inst. Sci and Tech.

KELLER, H. B. 1977 Numerical solution of bifurcation and nonlinear eigenvalue problems. In *Applications of Bifurcation Theory* (ed. P. H. Rabinowitz), pp. 359–384. Academic.

LEONARD, B. P. 1979 A stable and accurate convective modelling procedure based on quadratic upstream interpolation. *Comput. Meth. Appl. Mech. Engng.* **19**, 59–98.

NANDAKUMAR, K. & MASLIYAH, J. H. 1982 Bifurcation in steady laminar flow through curved tubes. *J. Fluid Mech.* **119**, 475–490.

NANDAKUMAR, K., MASLIYAH, J. H. & LAW, H.-S. 1985 Bifurcation in steady laminar mixed convection flow in horizontal ducts. *J. Fluid Mech.* **152**, 145–161.

ROACHE, P. J. 1976 *Computational Fluid Dynamics.* Hermosa.

RYSKIN, G. & LEAL, L. G. 1983 Orthogonal mapping. *J. Comput. Phys.* **50**, 71–100.

SCHAEFFER, D. G. 1980 Qualitative analysis of a model for boundary effects in the Taylor problem. *Math. Proc. Camb. Phil. Soc.* **87**, 307–337.

SIDI, A. 1991 Efficient implementation of minimal polynomial and reduced rank extrapolation methods. *J. Comp. Appl. Math.* in press. (Also *NASA TM*-103240, 1990.)

SOH, W. Y. 1988 Developing fluid flow in a curved duct of square cross section and its fully developed dual solutions. *J. Fluid Mech.* **188**, 337–361.

SOH, W. Y. & BERGER, S. A. 1987 Fully developed flow in a curved pipe of arbitrary curvature ratio. *Intl. J. Numer. Meth. Fluids* **7**, 733–755.

WINTERS, K. H. 1987 A bifurcation study of laminar flow in a curved tube of rectangular cross-section. *J. Fluid Mech.* **180**, 343–369.

WINTERS, K. H. & BRINDLEY, R. C. G. 1984 Multiple solutions for laminar flow in helically-coiled tubes. *Harwell Rep.* AERE R. 11373.

YANG, Z. H. & KELLER, H. B. 1986 Multiple laminar flows through curved pipes. In *Proc. Tenth Intl Conf. on Numerical Methods in Fluid Dynamics, Beijing, 1986* (ed. F. G. Zhuang & Y. L. Zhu). Lecture Notes in Physics, vol. 264, pp. 672–676. Springer.